On the efficiency of line-driving of AGN winds

Randall Dannen & Daniel Proga

University of Nevada, Las Vegas, Department of Physics & Astronomy

UNLV College of SCIENCES

Abstract

One of the main physical mechanisms that could drive mass outflows in AGN is radiation pressure on spectral lines. Although this mechanism is conceptually straightforward to understand, the actual magnitude of the radiation force is very challenging to compute because the force depends on physical conditions of gas and the strength, geometry, and SED of the radiation field. We present results from our photoionization and radiation transfer calculations of the radiation force using AGN type SEDs for both the ionizing and driving radiation fields. We use the photoionization code ***XSTAR*** and take into account the most up-to-date and complete atomic data and line list. We discuss implications of our results in the context of AGN winds that are observed in the UV and X-ray bands.

Introduction & Definitions

The force due to a single line can be many orders of magnitude greater than the force die to electron scattering alone. In order to determine the line force, we use the photoionization code ***XSTAR*** (Bautista & Kallman, 2001) to determine the equilibrium temperature for solar atomic abundances and an incident flux. To characterize the gas as we change the incident flux, it is useful to define a *photoionization parameter*, ξ,

$$\xi = \frac{4\pi F_X}{n_H}$$

To determine the line force, it is useful to define a normalized opacity, optical depth along with the traditional definitions (Stevens & Kallman 1990),

$$t = \frac{\sigma_e v_{th} \rho}{[dv/dr]}$$

$$\eta = \frac{\kappa_L}{\sigma_e}$$

$$\kappa_L = \frac{\pi e^2}{m_e c} g f \frac{N_L/g_L - N_U/g_U}{\rho \Delta \nu}$$

$$\tau_L = \eta t$$

Combining these definitions, we can determine the force multiplier, *M(t)*, due to all lines,

$$M(t) = \sum_{lines} \frac{\Delta\nu F_\nu}{F} \frac{1}{t}\Big[1 - \exp(-\eta t)\Big]$$

Then our expression for the total line force is,

$$f = M(t)\frac{F\sigma_e}{c}$$

Another important component to this calculation is the atomic data set. We use the latest versions of the atomic line list available from Robert Kurucz's database and merge it with the line list in ***XSTAR***. These two lists complement each other, Kurucz's list mostly contain lines in the IR to UV bands and ***XSTAR*** containing UV and X-ray lines. Our current line list contains approximately 2.5 million lines.

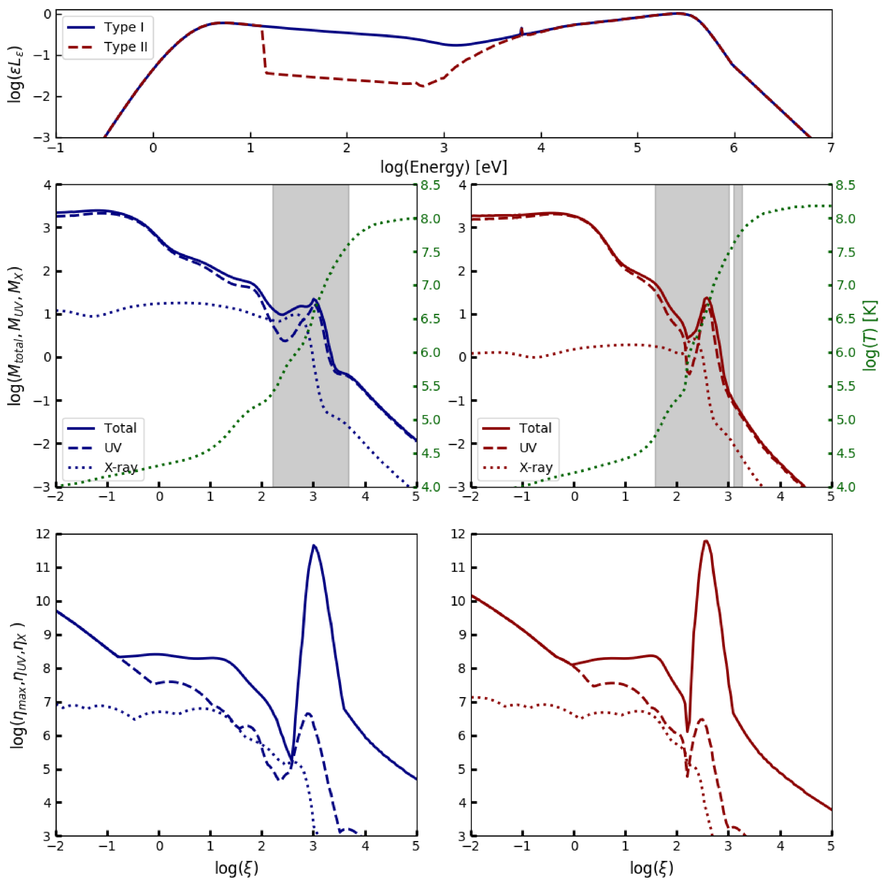

Current Results

In the above figure we summarize our current results. The top panel displays the two SED's, the type I in blue and type II in red (dashed) (Mehdipout et al, 2016). The colors in subsequent panels indicates which SED that information belongs.

The second panel displays the the force multiplier as a function of photoionization parameter with fixed optical depth parameter t = 10^{-6}. The green dashed line is the thermal equilibrium curve determined by ***XSTAR***, so as we change photoionization parameter, we are also varying temperature as well. The shaded areas on those figures indicate region that is unstable to isobaric perturbations. Previous works assumed that the majority of the line force came from UV (dashed) lines, but we wanted to address the question of how important X-ray lines (dotted) are for the total force multiplier. We see that at very highly ionized gas, X-ray lines become very important, providing the majority of the radiation force. Comparing this with previous results, such as those from Stevens & Kallman (1990), we find that our "bump" at log(ξ) ~ 3 to be much more pronounced, and we suspect this is due to our more complete atomic database. We also note that the X-ray contribution to the total force multiplier is a weak function of ξ until log(ξ) ~ 3.

The bottom two panels indicate the maximum line opacity (solid) and the maximum line opacity for UV (dashed) and X-ray (dotted) lines. The largest opacity happens to be for a very low energy line, in the IR band, it doesn't have a large impact on the total force multiplier, so it is important to have relatively opaque lines near the peak our spectral energy distribution in order to expect any significant effect from line driving.

Table Summary

	Type I			Type II	
$t = 10^{-6}$	$\log(\xi) \simeq 0$	$M_{total}(t) = 522$	$t = 10^{-6}$	$\log(\xi) \simeq 0$	$M_{total}(t) = 1635$
Ion	Wavelength (Å)	$M_L(t)$	Ion	Wavelength (Å)	$M_L(t)$
H I	1216	5.051	H I	1216	5.992
H I	1026	4.768	H I	1026	5.769
C IV	1550	1.550	C IV	1550	1.840
N V	1239	1.355	C III	977	1.562
O VI	1037	1.224	N V	1239	1.520
$t = 10^{-6}$	$\log(\xi) \simeq 1$	$M_{total}(t) = 123$	$t = 10^{-6}$	$\log(\xi) \simeq 1$	$M_{total}(t) = 117$
Ion	Wavelength (Å)	$M_L(t)$	Ion	Wavelength (Å)	$M_L(t)$
H I	1216	4.771	H I	1216	7.522
Ne VI	401	1.02	H I	1026	4.023
O VI	150	0.945	C IV	1548	2.227
O VII	21	0.724	N V	1239	1.907
C V	40	0.6812	O VI	1038	1.849
$t = 10^{-6}$	$\log(\xi) \simeq 2$	$M_{total}(t) = 24$	$t = 10^{-6}$	$\log(\xi) \simeq 2$	$M_{total}(t) = 9.2$
Ion	Wavelength (Å)	$M_L(t)$	Ion	Wavelength (Å)	$M_L(t)$
O VIII	19	0.604	H I	6563	0.409
Si X	303	0.399	O VI	1032	0.171
Fe XI	180	0.340	Fe XI	180	0.096
Fe XII	202	0.330	Fe X	174	0.089
Fe XIV	284	0.290	Fe XII	187	0.089
$t = 10^{-6}$	$\log(\xi) \simeq 3$	$M_{total}(t) = 20.03$	$t = 10^{-6}$	$\log(\xi) \simeq 2.6$	$M_{total}(t) = 22$
Ion	Wavelength (Å)	$M_L(t)$	Ion	Wavelength (Å)	$M_L(t)$
Fe XXIII	777	7.328	Fe XXIII	1157	6.200
Fe XXII	1157	3.546	Fe XXIII	1345	4.725
Fe XXII	1344	2.640	Fe XXIII	3739	3.909
Fe XXII	3738	2.172	Fe XXIII	9587	2.193
Fe XXII	9586	1.561	O VIII	1303	0.416

We show the five strongest unique lines for type I (left) and type II (right) AGN shown in the figure to the left.

Summary and future work

The next stages of this work will be to explore the dynamical consequences of the new radiation force, incorporating the results of our calculations into a magneto-hydrodynamic code and running simulations of disk winds and inflows from outflows in AGN. One of our expectations is that we might find two different stages of acceleration caused by the bumps the line force at high ionization parameter caused by Fe and O lines. In our new simulations we will use radiative heating and cooling rates that were computed also with ***XSTAR*** for the same SEDs (see Dyda et al. 2017). Therefore, our new gas dynamics simulation will have most up-to-date and complete line opacity and heating and cooling rates that are tailored to study objects with a given SED and chemical abundance.

We would like to thank Tim Kallman for his advice, time, and effort beginning this project with us.

References

- Bautista, M.A., Kallman, T.R., 2001, ApJ, 134:139-149
- Dyda, S., Dannen, R., Waters, T., & Proga, D. 2017, MNRAS 467, 4161-4173
- Mehdipour, M., Kaastra, J.S., Miller, M.C., et al., 2015, A&A 575:A22
- Stevens, I. R., & Kallman, T. R. 1990, ApJ, 365, 321

contact: dannenr@unlv.nevada.edu